16th Australasian Fluid Mechanics Conference
Crown Plaza, Gold Coast, Australia
2-7 December 2007

Upstream Influence of a Porous Screen on the Flow Field of a Free Jet

A.J. Neely[1] and J. Young[1]

[1]School of Aerospace, Civil and Mechanical Engineering
UNSW@ADFA, Canberra, ACT, 2600 AUSTRALIA

Abstract

This paper investigates the upstream influence of a range of transverse porous screen geometries on the flow fields of free jets. Infrared thermography was used to map the vertical distribution of temperature in a horizontal heated jet and measure the upstream influence of the screen. Two-dimensional CFD simulations of the flow fields of jets passing through a transverse porous screen, modelled as an array of cylindrical filaments, were also performed for a range of flow speeds (Re_D = 6847 to 54779) and screen porosities (β = 0.5 to 1). Reasonable agreement in flow behaviour was obtained using the two methodologies, both of which identified a spreading of the jet flow at the plane of the screen which was primarily dependent on the screen porosity and to a lesser degree the flow Reynolds number. The numerical simulations for these flow conditions predicted that, for a screen placed at x/D = 2, the increase in the full-width half-maximum of the jet velocity profile in the plane of the screen was less than 5% for porosities above 0.85 but increased an order of magnitude when the screen porosity was reduced to 0.5.

Introduction

A large body of work has been published on the influence of a porous screen on a flow field. Laws & Livesy [6] divided this work into three general categories, principally in reference to generating flow uniformity from a non-uniform free stream, or imposing a velocity distribution on a uniform free stream or finally on investigating the influence of the screen on the downstream turbulence level (e.g. [10], [3]). A number of investigators have also quantified the pressure drop across woven screens (e.g. [1], [12]).

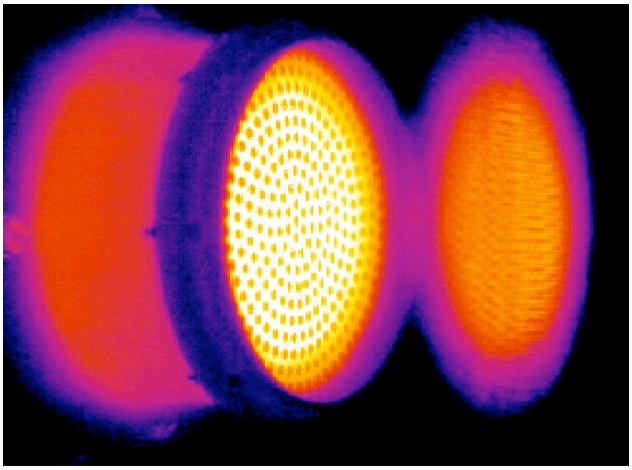

Figure 1. Mapping temperature distribution in the heated jet flow issuing from a perforated nozzle via IR using a high-emissivity porous screen placed transverse to the flow [9].

This previous work has concentrated on the downstream influence of a screen while little effort has been spent on examining the upstream influence of these screens on the flow. This aspect is of interest when porous screens are used to image the temperature distributions in a flow field, via infrared thermography (Figure 1) [9] or thermochromic liquid crystal thermometry [8].

Elder [2] and then Turner [11] considered the flow through non-uniform porous screens, which they referred to as gauzes, but their detailed analytical and numerical solutions were applied to ducted flows in which the flow could not spread laterally. Koo and James [4] similarly considered the case of a screen submerged in a ducted flow. Loudon and Davis [7] did investigate the divergence of flow approaching a submerged screen, in reference to the behaviour of a pectinate insect antenna. They observed a lateral "stretching" of the approaching flow field by factors of 5 and 10 times but again the flow was ducted and they only considered very low Reynolds numbers (Re_D = 0.5, 1, 3 based on duct height) and low porosities (β = 0.44, 0.09).

There is thus a need to quantify the degree of upstream flow distortion generated by the introduction of high porosity screens into an unbounded flow. This paper will discuss two approaches that have been used to investigate the upstream influence of porous screens on free jets, one experimental the other numerical.

IR Measurements of Flow Spreading

A variety of methods are available to the experimentalist to measure the spatial distribution of a flow field. These include traversing point or rake measurements of temperature and pressure, or the more precise but involved techniques of PIV, LDA and hot wire measurements.

The method of introducing an efficient emitter into a heated flow field was used here to visualise the upstream influence of the mesh on a free jet. A thin, matt-black, polyester ribbon was suspended end-on, under tension, vertically across the flow field of a heated free jet issuing from a hot air gun, approximately three nozzle exit diameters (D) downstream. A porous screen, placed transverse to the flow, was located at a range of downstream proximities to the trailing edge of the ribbon. The surface temperature distribution of the ribbon was then imaged by an IR camera and was taken to be indicative of the spread of the free jet. The low thermal conductivity and the reasonably low thermal mass of the ribbon ensure that the surface temperature of the ribbon closely follows the flow temperature, although some temporal smearing of any fluctuations can be expected. The presence of the ribbon itself introduces some flow field distortion but this is minimised for the small thickness (0.006D) and chord length (0.23D) of the ribbon and the fact that the relative change in observed jet width is the parameter measured.

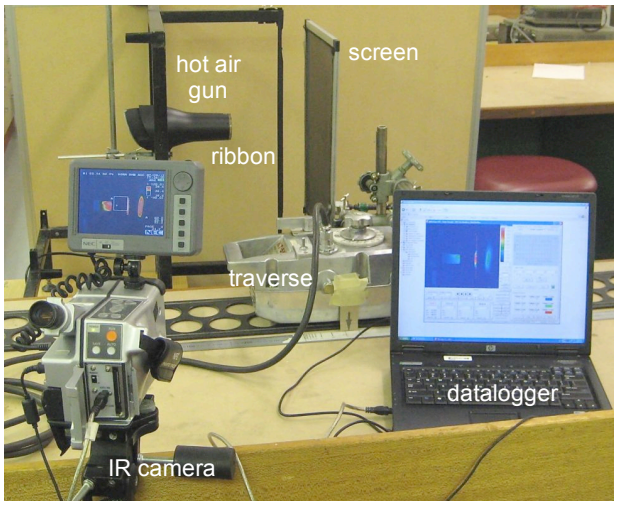

Figure 2. Experimental set up for the IR measurements of upstream influence of the screen on temperature profile of the jet from a hot air gun.

A transverse, porous, powder-coated, fine aluminium screen, of regular rectangular weave, with porosity of approximately $\beta = 0.8$, was gradually traversed from a location downstream into close proximity of the ribbon (Figure 2). Any change in the temperature distribution on the ribbon and thus the jet flow field due to the proximity of the screen downstream of the ribbon, was recorded by the IR camera. At each position the ribbon temperature was allowed to equilibrate for at least 60 seconds to account for any thermal inertia in the ribbon and the screen. An example history of ribbon surface temperature, measured during an experiment, shows the low level of fluctuations recorded, $< \pm 0.4$ °C (Figure 3). Again this was a function of both the fluctuations in the jet flow field and the thermal smoothing performed by the ribbon.

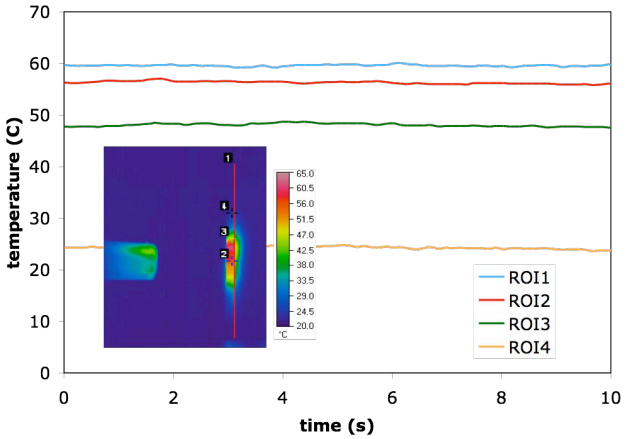

Figure 3. Temperature histories at a number of regions of interest (ROIs) on the ribbon.

Snapshots of the temperature distributions recorded by the IR camera are collected in Figure 4, clearly showing the play of the thermal plume on the ribbon and the transverse screen (viewed at an angle). In this case the ribbon was located slightly off-centre of the plume to avoid the thermal wake from a strut in the exit nozzle of the hot air gun. A slight broadening of the plume on the trailing edge of the ribbon is discernable as the proximity of the screen increases. In the first image the nozzle of the hot air gun is retained to indicate its relative position to the ribbon. This position was held constant throughout the tests. In the first image the screen is seen to be immediately downstream of the trailing edge of the ribbon. In the subsequent images it is gradually traversed downstream of the ribbon until the final image where it is no longer present.

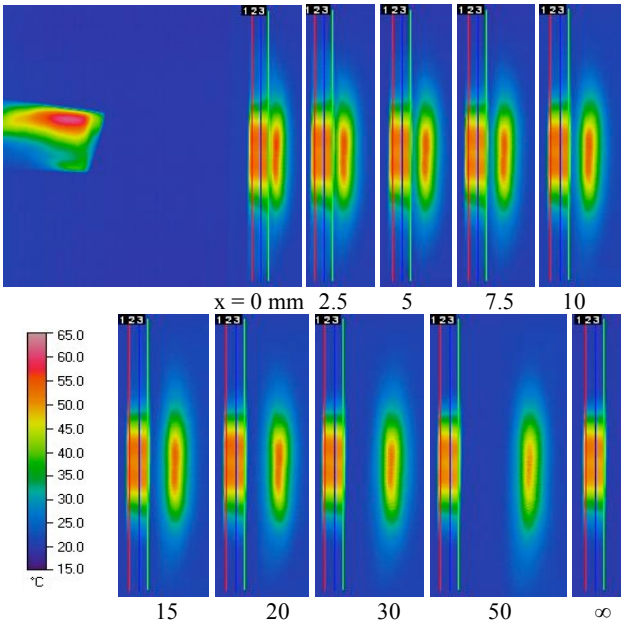

Figure 4. IR images of the ribbon, heated by the jet from a hot air gun, as the screen is traversed downstream from the trailing edge of the ribbon.

This process was repeated for a number of flow speeds (U_{exit} = 10, 15 m/s) and flow temperatures (T_{exit} = 45, 65 ºC). Vertical line distributions along the ribbon were extracted from the IR images and compared for different screen proximities. Figure 5 plots these temperature distributions for the trailing edge of the ribbon. The asymmetric nature of the temperature field is due to the presence of a horizontal struts in the exit nozzle of the hot air gun and the effect of buoyancy in the flow. It can be seen that there is a small but distinct spreading of the jet flow field induced by the screen. This is apparent when each distribution is compared to that with no screen present (proximity = 300 mm).

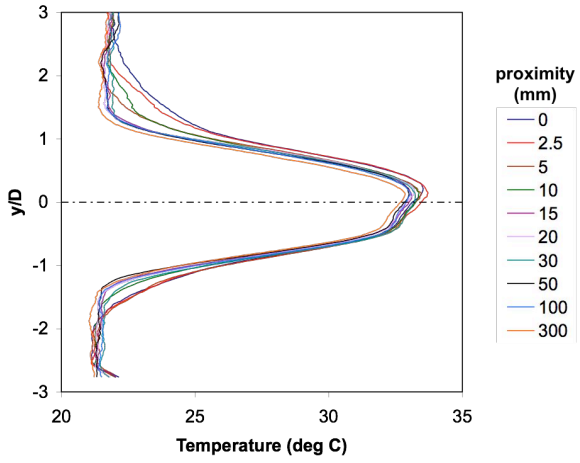

Figure 5. Smoothed temperature distributions in 45 ºC jet, upstream of screen for a range of proximities.

There are a range of metrics that can be used to measure jet spread. The most common is the full-width half-maximum (FWHM) or jet half-width measure applied to the transverse velocity distribution in the jet [5].

To quantify the upstream influence of the screen on the flow field, the FWHM was calculated for each proximity at the trailing edge of the ribbon. These values are plotted in Figure 6 in which the FWHM values are nondimensionalised by dividing them by the value for no screen present.

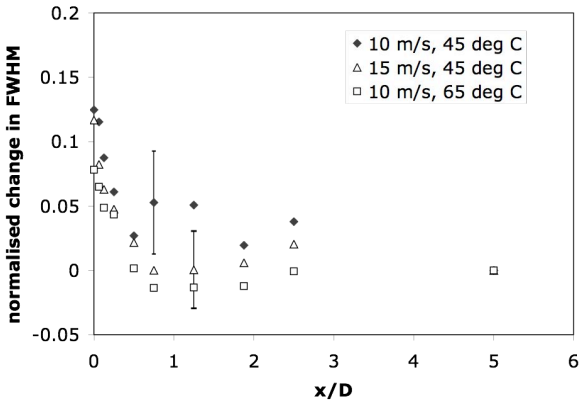

Figure 6. Full-width half-maximum of the jet flow temperature distribution as a function of the downstream proximity of the porous screen (β=0.8) for a range of jet exit velocities and temperatures.

The transient variation of the temperature distribution on the ribbon was measured by recording 10 second IR image sequences at 10 Hz. The observed point temperature variation was up to 0.8 ºC (Figure 3), which was more likely to be indicative of the turbulence in the plume of the hot air gun than of any temperature variation at the source itself. This uncertainty in temperature was used to generate the error bars shown in Figure 6 and largely explains the scatter seen in the data points with a higher level of uncertainty for the lower temperature flows due to a decrease in IR signal level compared to the ambient level.

A number of trends can be seen within the experimental scatter of the data. Over the limited parametric range examined, the jet spreading is observed to decrease slightly as Re_D increases. Also the upstream influence of the screen increases with increasing proximity, as expected. Distortions in the flow field of about 8-12% of the FWHM were observed at the closest proximity, which decreased to < 5% FWHM at x = 0.2D from the screen. Thus the noticeable upstream flow distortion is confined to a region close to the screen.

Numerical Investigation of Flow Spreading

In order to investigate the upstream spreading of a jet as it approaches a porous screen, in more detail, a two-dimensional model problem was examined via CFD using the Fluent commercial flow solver. Although the physical flow interaction of interest is three-dimensional in nature, for this initial numerical study it was felt that the simplicity of a 2D solution was warranted. An axial symmetry plane through the centre of the jet was used to further reduce the 2D problem. An axisymmetric solution was not possible due the need to recreate a uniform porosity while maintaining a regular spacing between filaments in the screen. The Fluent solver does permit the use of a porous wall that could help to overcome this limitation and enable axisymmetric solutions but it was desired here to investigate the interaction with individual filaments in the screen. It is believed that the two dimensional approach is conservative as it only allows spreading in two directions and we therefore may expect less jet distortion in the actual 3D case.

A plane jet source, modelled as a velocity inlet, was placed a distance of two jet diameters upstream of an array of cylinders, as shown schematically in Figure 7. The transverse array of cylinders was extended to a distance of 2.25D from the centreline. This was initially done to represent a nominally infinite screen extent. It was later observed from the CFD simulations that the presence of the screen away from the jet core does in fact influence the local entrainment of flow into the jet however this influence on the jet behaviour is felt to be negligible given the extremely small flow velocities induced this far from the jet.

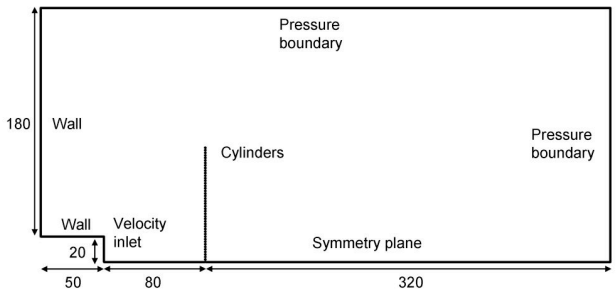

Figure 7. Schematic of the computational domain (dimensions in mm).

The flow was assumed to be steady and incompressible. It was modelled with second-order upwind spatial discretisations, and pressure-velocity coupling through the SIMPLE algorithm. The jet was assumed to be fully turbulent, using the Spalart-Allmaras turbulence model with a characteristic length equal to 0.07D where D is the jet exit width (40 mm), and 10% turbulence intensity. This value was chosen arbitrarily to model the likely turbulence levels from the hot air gun, but was not measured directly.

A number of different flow configurations were investigated, including varying the jet exit velocity profile between uniform (*top hat*) and parabolic, and the maximum jet velocity at exit (2.5, 5.0, 10.0, 20.0 m/s). These values were chosen to bound the likely jet flows and velocity distributions found in practical cases to which the IR screen technique might be applied. In addition varying porosities of the screen were considered (β = 0.85, 0.75, 0.5) by varying the cylinder diameter while maintaining the spacing between their centres at 0.05D. In each case the flow was also calculated with no screen present, for reference.

Calculations were performed on a mixed quadrilateral-triangular grid with 287,560 cells, 40 grid points across the jet inlet half-width, 48 points around the cylinders, and values of y+ < 0.9 on the cylinder surfaces (Figure 8). Subsequent calculations on a grid with twice the resolution in each direction (1,150,240 cells, 80 grid points across the jet inlet half-width, 96 points around the cylinders) for one of the cases (parabolic jet exit profile, 10 m/s maximum jet velocity, β = 0.85) showed negligible variation in jet spread (< 0.2% variation in the difference in FWHM with and without the screen present). Halving the resolution (71,890 cells, 20 grid points across the jet inlet half-width, 24 points around the cylinders) resulted in a 3% change in jet spread. Accordingly the initial grid was considered sufficient for the remainder of the calculations.

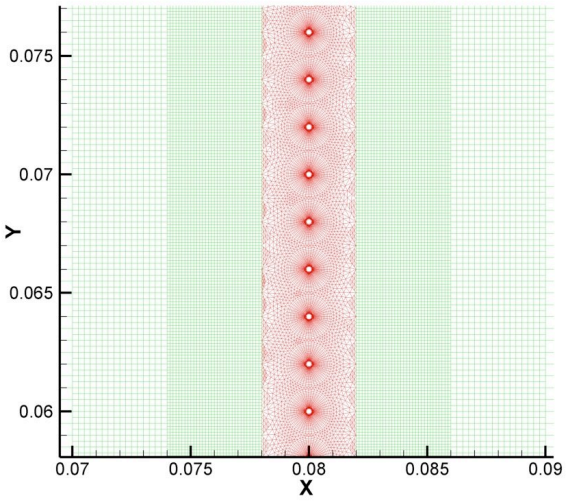

Figure 8. Detail of the distribution of CFD grid cells around the cylindrical array representing the screen.

Jet spread was evaluated by calculating the FWHM of the horizontal velocity profile at the centreline of the cylinder array, representing the screen, vertically across the domain, and determining the relative change from the no-screen case. As the flow approaches the gaps between the cylinders it speeds up relative to the local flow velocity, and this, in addition to the boundary layers on the cylinders, results in a very non-uniform velocity profile in the plane of the screen. Accordingly the horizontal velocity was measured only at the midpoints of the gaps between the cylinders (Figure 9), and this profile interpolated (using cubic splines) to provide a nominal velocity at the symmetry plane (where there is a cylinder). This velocity profile was then used to determine the FWHM.

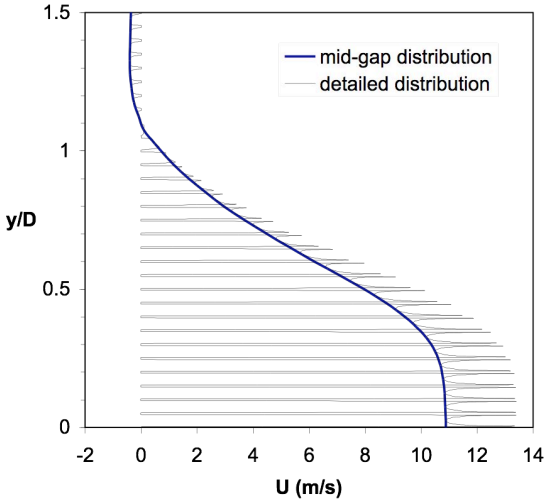

Figure 9. Velocity distribution sampled at the plane of the screen at the mid-gaps of the cylinder array (β=0.85) for the jet with top hat jet exit velocity profile (Re_D = 27390).

The extracted velocity profiles for the top hat and parabolic jets are mirrored about the jet centreline and plotted in Figures 10 and 11 showing the spreading of the jets as the porosity of the screen is decreased. The velocity profile generated at higher grid density is also plotted in Figure 11 demonstrating the grid independence of the solution.

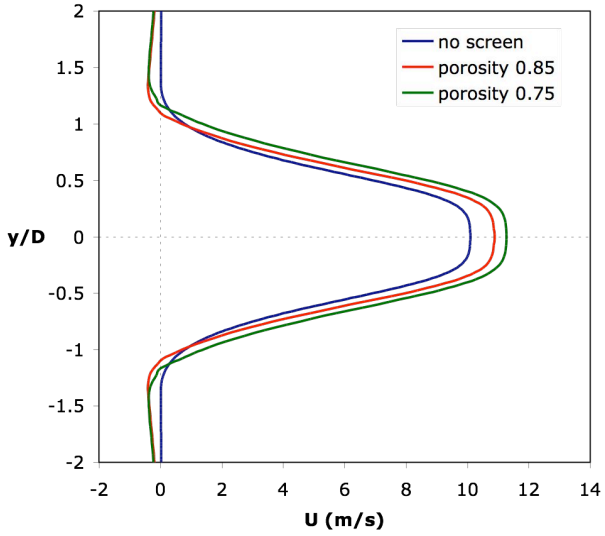

Figure 10. Comparison of velocity profiles at the plane of the screen for a range of porosities at Re_D = 27390 and a top hat jet exit velocity profile. (Velocities sampled at screen array gap midpoints).

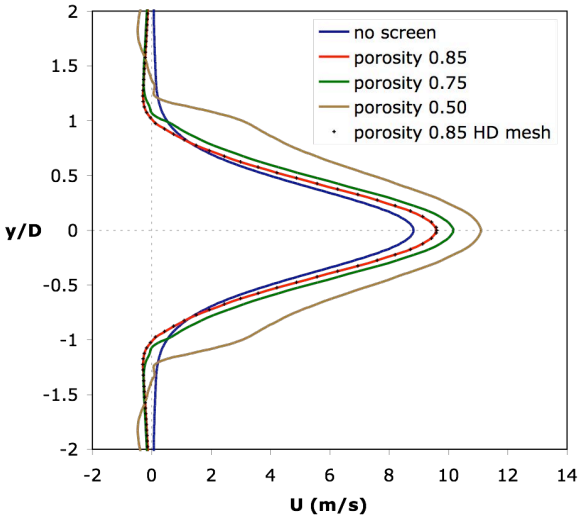

Figure 11. Comparison of velocity profiles at the plane of the screen for a range of porosities at Re_D = 27390 and a parabolic jet exit velocity profile. (Velocities sampled at screen array gap midpoints). HD indicates the high density computational mesh.

The normalised change in FWHM at the plane of the screen was correlated against porosity of the screen (Figure 12) and the Reynolds number, based on the jet exit diameter (D), of the approaching flow in the jet (Figure 13). The jet spreading is, as expected, a strong inverse function of the screen porosity. A 50% increase in the FWHM of the jet is predicted at the screen plane for a screen porosity of 0.50, due to the high blockage, but this falls to approximately 4% when the porosity is increased to 0.85. The extreme case of this behaviour would be the total spreading of a jet impinging on a non-porous plate. The spread of the jet with the top hat velocity distribution is predicted to be greater than that for the jet with the parabolic velocity profile, possibly due to the higher mass flow rate in the top hat case.

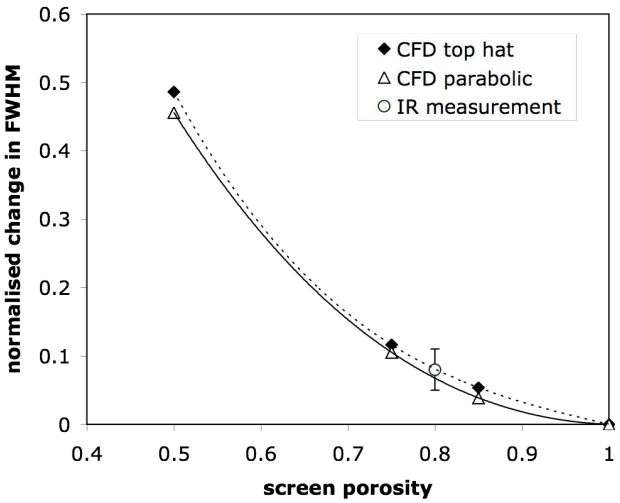

Figure 12. Variation in FWHM with screen porosity for jet Re_D = 27390 for both the top hat and parabolic exit velocity profiles.

The degree of jet spread deduced from the temperature distributions measured in the IR experiments at the plane of the porous screen is also shown in Figure 12 for comparison, and is seen to be in good agreement with the CFD predictions.

The correlation between the degree of jet spreading and the flow Reynolds number is shown in Figure 13. As Re_D increases, the degree of jet spreading is predicted to decrease. This dependency is stronger for the lower Reynolds numbers considered and is no

longer significant at the higher end of the Reynolds number range. This is to be expected due to the decrease in boundary layer thickness relative to the cylinder diameter as Re_D increases lowering the effective blockage of the screen. The greater spreading experienced by the jet with the top hat exit velocity profile is more apparent in this figure.

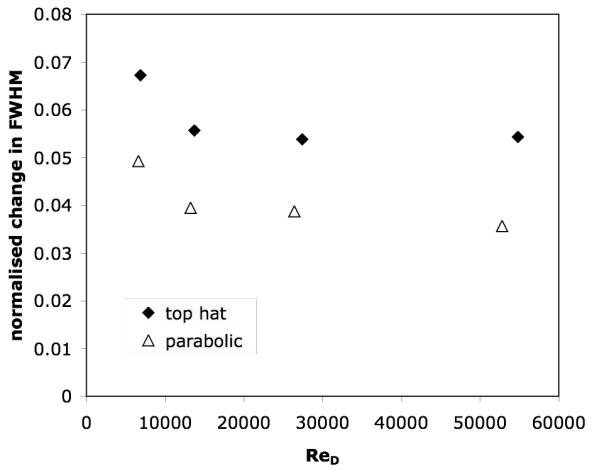

Figure 13. Variation in FWHM with Re_D for the jets with top hat and parabolic exit velocity profiles ($\beta = 0.85$).

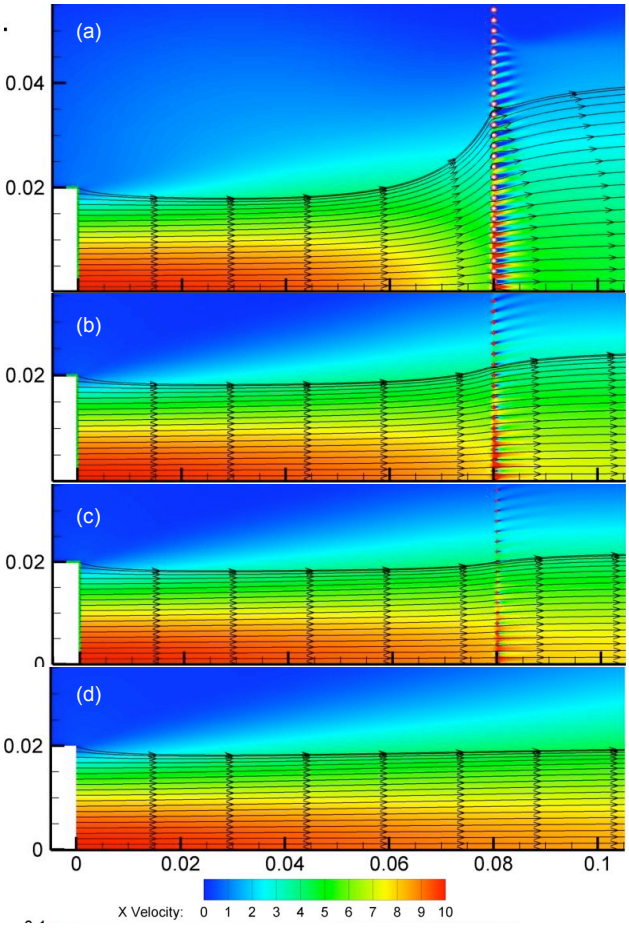

Figure 14. Flow field distortion of a parabolic jet (Re_D = 27390) upstream of screens of varying porosity: (a) β=0.50, (b) β=0.75, (c) β =0.85 and (d) no screen. (contours of x-velocity in m/s, axis dimensions in m)

As another measure of the upstream influence of the screen, streamlines were tracked downstream from the jet exit to visualise the relative spreading of the jet at different screen porosities. This is analogous to the metric used by Loudon & Davis [7] to measure the spread around their porous insect antenna.

For the flow from the jet with parabolic exit velocity profile and Re_D = 27390 shown in Figure 14 it can be clearly seen that the disturbance caused by the β = 0.85 screen is minimal but increases significantly when the porosity of the screen is decreased to β = 0.50. The region of flow disturbance is also observed to extend further upstream as the screen porosity is decreased.

To quantify the extent of the upstream influence of the screen, velocity profiles were extracted in transverse planes spaced between the jet outlet and the screen location. These profiles are compared in Figure 15 and Figure 16 to the matching profiles for the undisturbed jets.

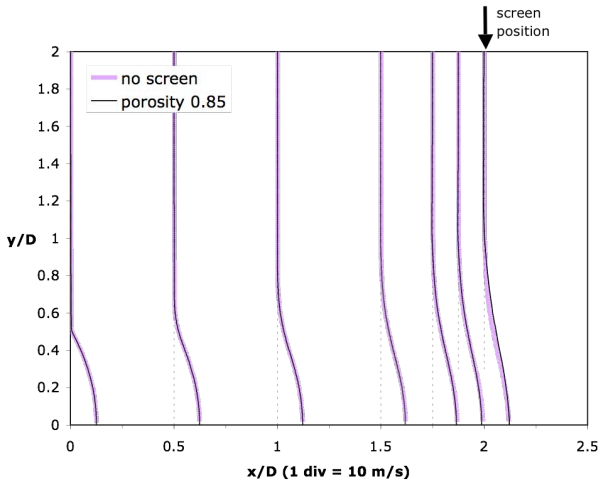

Figure 15. Comparison of CFD predictions of the velocity profiles in the parabolic jet at Re_D = 13199 with and without the presence of a screen (β = 0.85).

It can be seen that for both the jets with parabolic and top hat exit profiles, the discernible influence of the (β = 0.85) screen on the velocity profile extends less than 0.25D upstream which is consistent in trend, if not level with the IR ribbon experiments.

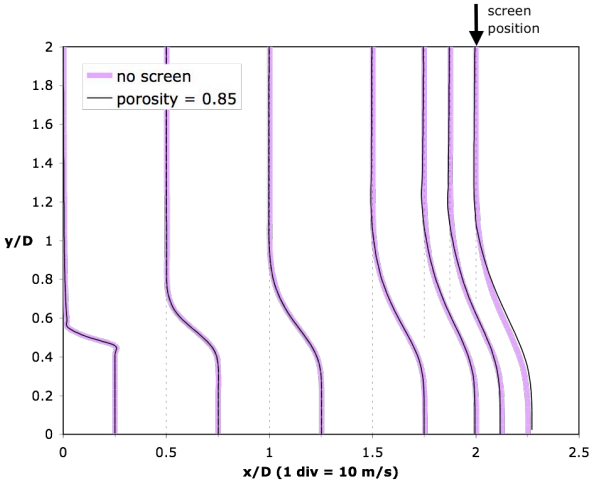

Figure 16. Comparison of CFD predictions of the velocity profiles in the top hat jet at Re_D = 26397 with and without the presence of a screen (β = 0.85).

The streamlines at half the jet exit radius and the full jet exit radius were tracked to determine the spreading of the jet streamtubes in the presence of a porous screen. The transverse positions of these bounding streamlines were measured at the plane of the screen and compared with the no-screen case. These measurements of spreading were normalised against the undisturbed stream tube positions and are compared in Figure 17 for a range of Re_D and porosities. To avoid misleading scatter in this data, where a streamline was grossly disturbed by the presence of a screen filament, the undisturbed position of the streamline was interpolated from the streamline directions a few filament diameters upstream and downstream of the screen.

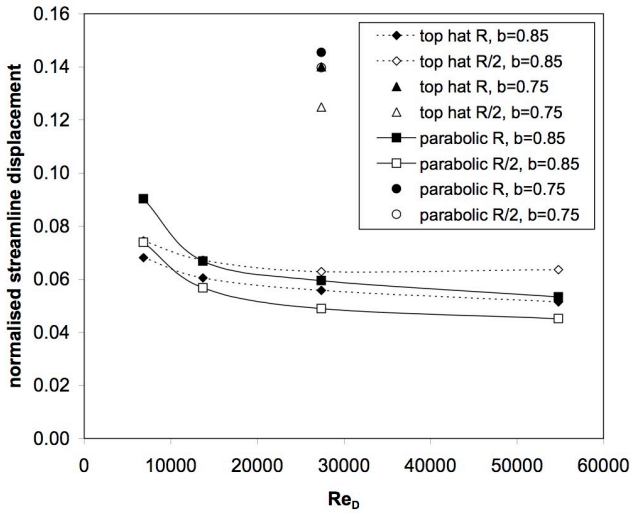

Figure 17. CFD predictions of jet stream tube widening as a function of Re_D, at half jet exit radius (R/2) and full jet exit radius (R) for a range of velocity distributions and screen porosities.

A similar trend in the upstream distortion of the jet flowfield is observed using this metric as that obtained from the comparison of FWHM of the jet with an initially strong inverse dependence decreasing in strength with Re_D. The upstream spatial distortion decreases with increasing flow Re_D due to the thinning boundary layers around the screen filaments, to a level of approximately 5% - 7% at the higher values of Re_D which is slightly higher than the values predicted from the FWHM. There is again a difference in the magnitude of this distortion for the two jet velocity profiles examined with the jet with top hat exit velocity profile spreading more than that with parabolic exit velocity profile.

Some difference in the degree of jet spread may be expected between the experimental measurements in the heated three-dimensional jet and the cold two-dimensional simulations although the agreement observed is reasonable.

It is intended to extend this computational modelling to a greater range of porosities and flow speeds. To increase the accuracy of the modelling it will also be necessary to move to full 3D modelling to capture both the axisymmetric nature of the jet and the regular repetitive geometry of the screen. It would also be useful to model the temperature distribution and any buoyancy effects in the jet, to more accurately determine the spatial inaccuracy of temperature distributions mapped using porous screens.

Conclusions

The extent of the disturbance to the flow field of a free jet induced upstream of a porous screen has been quantified numerically and experimentally for a limited number of cases. Reasonable agreement in flow behaviour was obtained using the two methodologies, both of which identified a spreading of the jet flow at the plane of the screen which was primarily dependent on the screen porosity and to a lesser degree the flow Reynolds number.

The two dimensional CFD solutions indicated a minimal spreading of the jet (4-6% of the FWHM) at the plane of the screen for porosities of 0.85 or higher with the flow distortion extending approximately 0.25 jet diameters upstream. The upstream flow distortion induced by the screen was predicted to increase significantly for lower screen porosities (50% of the FWHM for $\beta = 0.50$) and lower approach Reynolds numbers.

The thermographic maps of upstream temperature distribution indicated a slightly greater degree of jet spreading (10-12% of the FWHM for $\beta = 0.80$) with this influence extending further upstream than predicted by the CFD, as may be expected at the lower porosity examined. More detailed experimental measurements using laser Doppler anemometry are desirable to fully validate the numerical predictions.

The experimental and numerical results reported in the present study indicate that the upstream influence of a porous screen on the flow of a jet can be minimised, when used as an intrusive flow diagnostic, by using screens with porosities greater than 85%.

References

[1] Armour, J.C. & Cannon, J.N., Fluid flow through woven screens, *AIChE J.,* **14**, 1968, 415-420.

[2] Elder, J.W., Steady flow through non-uniform gauzes of arbitrary shape, *J. Fluid Mech*., **5**, 1959, 355-368.

[3] Groth, J. & Johansson, A.V., Turbulence reduction by screens, *J. Fluid Mech*., **197**, 1988, 139-155.

[4] Koo, J.-K. & James, D.F., Fluid flow around and through a screen, *J. Fluid Mech*., **60**, 1973, 513-538.

[5] Kotsovinos, N.E., A note on the spreading rate and virtual origin of a plane turbulent jet, *J. Fluid Mech*., **77**, 1976, 305-311.

[6] Laws, E.M. & Livesey, J.L., Flow Through Screens, *Ann. Rev. Fluid Mech.*, **10**, 1978, 247-266.

[7] Loudon, C. & Davis, E.C., Divergence of streamlines approaching a pectinate insect antenna: consequences for chemoreception, *J. Chem. Ecol*., **31**, 2005, 1-13.

[8] Mee, D.J., Ireland, P.T., & Bather S., Measurement of the temperature field downstream of simulated leading-edge film-cooling holes, *Exp. Fluids*, **27**, 1999, 273–283.

[9] Neely, A.J., Measurement of gas temperature distributions in flows using radiating high-porosity meshes, in *Proceedings of the 5th Pacific Symposium on Flow Visualisation and Image Processing*, editor Milton, B., 2005.

[10] Taylor, G.I. & Batchelor, G.K., The effect of wire gauze on small disturbances in a uniform stream, *Q. J. Mech. Appl. Maths*, **2**, 1949, 1-29.

[11] Turner, J.T., A computational method for the flow through non-uniform gauzes: the general two-dimensional case., *J. Fluid Mech*., **36**, 1969, 367-383.

[12] Wu, W.T., Liu, J.F., Li, W.J. & Hsieh, W.H., Measurement and correlation of hydraulic resistance of flow through woven metal screens, *Int. J. Heat Mass. Tran.,* **48**, 2005, 3008-3017.